

Tuning the interaction between propagating and localized surface plasmons for surface enhanced Raman scattering in water for biomedical and environmental applications

Masahiko Shioi, Hilde Jans, Kristof Lodewijks, Pol Van Dorpe, Liesbet Lagae, and Tatsuro Kawamura

Citation: [Applied Physics Letters](#) **104**, 243102 (2014); doi: 10.1063/1.4883743

View online: <http://dx.doi.org/10.1063/1.4883743>

View Table of Contents: <http://scitation.aip.org/content/aip/journal/apl/104/24?ver=pdfcov>

Published by the [AIP Publishing](#)

Articles you may be interested in

[Sensitive surface-enhanced Raman scattering active substrate based on gap surface plasmon polaritons](#)

J. Vac. Sci. Technol. B **32**, 012601 (2014); 10.1116/1.4862161

[Application of EBL fabricated nanostructured substrates for surface enhanced Raman spectroscopy detection of protein A in aqueous solution](#)

J. Vac. Sci. Technol. B **31**, 06F901 (2013); 10.1116/1.4821800

[Multimodal plasmon coupling in low symmetry gold nanoparticle pairs detected in surface-enhanced Raman scattering](#)

Appl. Phys. Lett. **98**, 183115 (2011); 10.1063/1.3555429

[Tuning plasmonic interaction between gold nanorings and a gold film for surface enhanced Raman scattering](#)

Appl. Phys. Lett. **97**, 163106 (2010); 10.1063/1.3504187

[Ultradense gold nanostructures fabricated using hydrogen silsesquioxane resist and applications for surface-enhanced Raman spectroscopy](#)

J. Vac. Sci. Technol. B **27**, 2640 (2009); 10.1116/1.3253610

Agilent's Electronic Measurement Group is becoming **Keysight Technologies**.

Engineering Education & Research Resources DVD 2014

Agilent is the key to your test and measurement needs **Order yours**

Agilent Technologies

Tuning the interaction between propagating and localized surface plasmons for surface enhanced Raman scattering in water for biomedical and environmental applications

Masahiko Shioi,^{1,2,a)} Hilde Jans,³ Kristof Lodewijks,^{3,4} Pol Van Dorpe,^{3,5} Liesbet Lagae,^{3,5} and Tatsuro Kawamura¹

¹Device Solutions Center, Panasonic Corporation, 3-4, Hikaridai, Seika-cho, Soraku-gun, Kyoto 619-0237, Japan

²Department of Electric and Electronic Engineering, Graduate School of Engineering, Kobe University, Rokkodai, Nada, Kobe 657-8501, Japan

³Interuniversity Microelectronics Center VZW., Kapeldreef 75, 3001 Leuven, Belgium

⁴Department of Electrical Engineering, Katholieke Universiteit Leuven, Celestijnenlaan 200 D, B-3001 Leuven, Belgium

⁵Department of Physics, Katholieke Universiteit Leuven, Celestijnenlaan 200 D, B-3001 Leuven, Belgium

(Received 26 March 2014; accepted 4 June 2014; published online 16 June 2014)

With a view to biomedical and environmental applications, we investigate the plasmonic properties of a rectangular gold nanodisk array in water to boost surface enhanced Raman scattering (SERS) effects. To control the resonance wavelengths of the surface plasmon polariton and the localized surface plasmon, their dependence on the array period and diameter in water is studied in detail using a finite difference time domain method. A good agreement is obtained between calculated resonant wavelengths and those of gold nanodisk arrays fabricated using electron beam lithography. For the optimized structure, a SERS enhancement factor of 7.8×10^7 is achieved in water experimentally. © 2014 AIP Publishing LLC. [<http://dx.doi.org/10.1063/1.4883743>]

Surface enhanced Raman scattering (SERS) is strongly enhanced Raman scattering from molecules adsorbed on the surface of metallic nanostructures that exhibit local surface plasmon resonances. SERS has received considerable attentions in recent years because of its high sensitivity down to the single-molecule detection limit in specific molecules.¹⁻³ The enhancement mainly arises from enhanced local electromagnetic (EM) fields due to surface plasmon resonances.⁴ Additionally, chemical interactions between adsorbed molecules and metallic nanostructures may provide an additional enhancement due to charge transfer between metal and molecules. Because of its high sensitivity, SERS is a promising powerful tool for biomedical and environmental sensing, e.g., blood glucose detection,⁵ virus detection,⁶ arsenic detection in contaminated water,⁷ and the detection of chemical pollutants in sea-water such as polycyclic aromatic hydrocarbon.⁸

The enhancement factor (EF) of SERS depends on EM-field intensities at excitation and detection wavelengths.^{4,9} To maximize EFs, EM-field intensities at both excitation and detection wavelengths should be strongly enhanced. A double-resonance substrate has been proposed and demonstrated as one of the most promising structures to achieve maximized intensities at both excitation and Raman wavelengths.¹⁰⁻¹⁴ In general, a double-resonance substrate consists of an array of gold (Au) nanoparticles or nano-disks and a continuous gold film separated by a dielectric spacer. It supports surface plasmon polaritons (SPPs) and localized surface plasmons (LSPs) simultaneously. SPPs and LSPs are strongly coupled and two hybridized modes are observed.¹³

By tuning the structural parameters, a double-resonance substrate provides a SERS EF of 8.4×10^8 in air for a silver arrays and 7.2×10^7 in Au nano-disk arrays.¹³

For biomedical and environmental applications of SERS, excitations in the near infrared (NIR) region are suitable because of the smallness of the interaction of NIR light with biological media.^{5,14-16} In many applications, e.g., *in-situ* detection of biomolecules,^{17,18} blood glucose measurements,¹⁹ pharmaceutical chemicals detection in water,²⁰ and aromatic chemical detection in sea water,²¹ SERS is measured in water. In this Letter, we first calculate the electric field for a model representing double-resonance substrates, based on Au nano-disk arrays placed in water, by a finite-difference time-domain (FDTD) method to match the grating constant of the nano-disks array to excite SPPs in water and to tune the diameter of Au nano-disks for controlling the LSP resonance wavelength by taking into account the refractive index of water. From calculation results, we fabricated double-resonance substrates using electron beam lithography. We show that tuning of the interaction between SPPs and LSPs by controlling the pitch of the Au nano-disk in the directions parallel and perpendicular to the polarization of the excitation light results in an EF as large as 7.8×10^7 in the NIR region in water.

Figure 1(a) shows a schematic illustration of a double-resonance substrate. An Au nano-disk array is formed on an Au film with a SiO₂ spacer. A thin titanium (Ti) film between the Au film and a quartz substrate serves as adhesion layer. For the preparation of the structure, a quartz substrate was cleaned in a sulfuric acid/hydrogen peroxide solution (H₂SO₄ (96%):H₂O₂ (30%) = 3:1) for 15 min followed by an oxygen plasma treatment. Ti(10 nm), Au(100 nm), and silicon dioxide (SiO₂) (30 nm) layers were

^{a)}Author to whom correspondence should be addressed. Electronic mail: shioi.masahiko@jp.panasonic.com. Tel.: +81-774-98-2556.

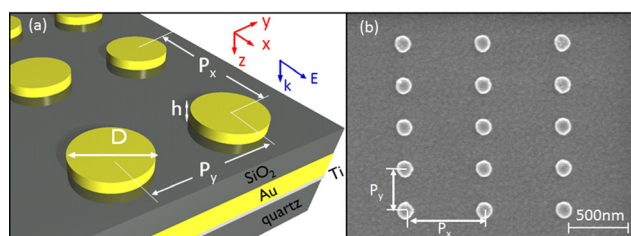


FIG. 1. (a) Schematic illustration of double-resonance gold nano-disk array substrate. (b) Scanning electron microscope image of a gold nano-disk array.

sputtered onto the cleaned substrate. A 200 nm polymethyl methacrylate (PMMA) resist layer was then spin-coated onto the substrate and nanodisk arrays were exposed by electron beam lithography. Development of the PMMA resulted in the formation of nanohole arrays in the PMMA layer. Au (30 nm) was then deposited to form nanodisks inside the holes. Finally, the PMMA layer was lifted off in acetone at 50 °C. Figure 1(b) shows a scanning electron microscope image of an Au nanodisk array. The overall size of the gold disk array is $100 \times 100 \mu\text{m}$ [Fig. 1(b)].

The optical response of the structure was calculated by a FDTD method (FDTD solutions, Lumerical Solutions, Inc., Vancouver, Canada). A metallic nanodisk array was illuminated with a plane wave at normal incidence, which propagates in the k -direction [Fig. 1(a)]. The electric field E was directed along the x -direction; see Fig. 1(a). Periodic boundary condition was used. The simulation region was $P_x \times P_y \times 1920 \text{ nm}^3$ with a non-uniform mesh, where P_x and P_y were the nanodisk pitches in x - and y -directions, respectively, in Fig. 1(a). For fine simulations around the nano-disks, $200 \times 200 \times 1920 \text{ nm}^3$ regions were calculated with a mesh size of 2 nm. The thickness of the quartz substrate was set to 2000 nm, and those of the SiO_2 , Ti, and Au films were 30, 10, and 100 nm, respectively. The height of the Au nano-disk was 30 nm. P_x and P_y were changed from 540 to

630 nm and from 200 to 400 nm, respectively. The refractive index of the background was set to 1.33 (water) and those of other materials were obtained by fitting the empirical Au,²² SiO_2 ,²³ and Ti²⁴ dispersion data with Lumerical's multi-coefficient model.²⁵

To measure the reflectance and SERS in water, the double-resonance substrates were mounted in a home-made flow cell with a 1-mm-thick cavity. Water was sent into the cell by a peristaltic pump. For reflectance measurements, $10\times$ objective (numerical aperture (NA): 0.2) was used for irradiation and detection. The polarization of the incident light was set parallel to the x -direction in Fig. 1(a). An area without nano-disks, i.e., a SiO_2 -coated Au film, was used as a reference. For SERS measurements, 4-aminothiophenol (4-ATP) was employed as a Raman probe. A monolayer of 4-ATP molecules was adsorbed onto nano-disks by soaking in a 1 mM ethanol solution overnight. Raman spectra were excited via $10\times$ objective (NA = 0.2) using a 785-nm diode laser (2.5 mW) and recorded by a LabRam HR 800 spectrometer (Horiba Jobin Yvon). Raman peaks in the $600\text{--}1800\text{-cm}^{-1}$ region, corresponding to wavelengths 824–915 nm, were studied.

Figure 2(a) presents a contour plot of calculated reflectance as a function of P_x and the wavelength. P_y and the nano-disk diameter are set to 300 nm and 130 nm, respectively. Two modes corresponding to SPP and LSP can be seen. SPP shifts to shorter wavelengths as P_x decreases. This occurs as a result of the matching of wave vectors for light and SPP (k_{spp}). In the double-resonance structure, k_{spp} is inversely proportional to P_x , specifically $2\pi/P_x$.²⁶ Fig. 2(a) indicates that the largest enhancement of the excitation field (785 nm) in water is achieved when P_x is 580 nm. Similar data, when P_y is changed, are shown in Fig. 2(b). P_x and the nano-disk diameter are set to 580 nm and 130 nm, respectively. The SPP resonant wavelength is almost independent of P_y , whereas that of the LSP moves to longer wavelength

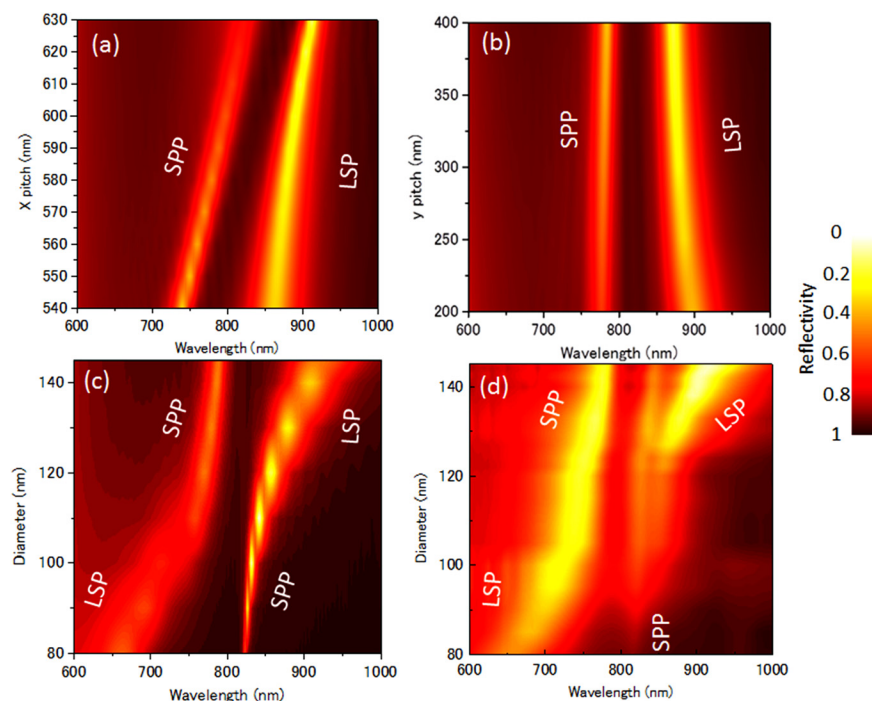


FIG. 2. Contour plots of calculated reflectance as functions of (a) P_x and wavelength ($P_y = 300 \text{ nm}$, diameter = 130 nm), (b) P_y and wavelength ($P_x = 580 \text{ nm}$, diameter = 130 nm), and (c) diameter and wavelength ($P_x = 580 \text{ nm}$, $P_y = 300 \text{ nm}$). (d) Contour plot of experimentally obtained reflectance as a function of diameter and wavelength ($P_x = 580 \text{ nm}$ and $P_y = 300 \text{ nm}$).

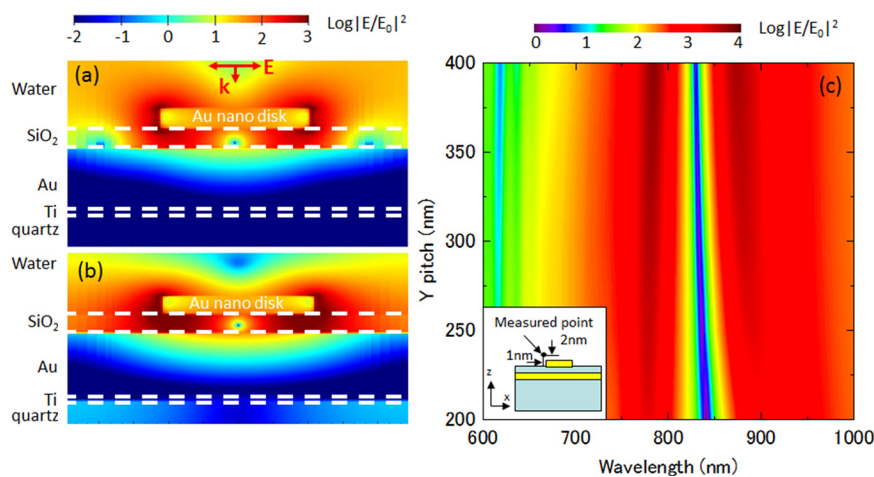


FIG. 3. Simulated electric field distributions for the structure with $P_x = 580$ nm, $P_y = 300$ nm, and $d = 130$ nm at (a) 785 nm (SPP resonance) and (b) 879 nm (LSP resonance). (c) Contour plot of electric field intensity as functions of P_y and wavelength ($P_x = 580$ nm).

and becomes broader as P_y decreases. This is because of the coupling between neighboring nano-disks in the y -direction, and resultant damping of the LSP resonance.²⁷

Figure 2(c) shows a contour plot of calculated reflectance in water as a function of diameter (80–145 nm) and the wavelength. P_x and P_y are set to 580 nm and 300 nm, respectively. The anti-crossing behavior is clearly seen.¹² Figure 2(d) shows experimentally obtained reflectance for the structure in Fig. 1(b). The experimental and calculated results agree very well except for a small reflection dip around 820 nm in the experimental data. This is caused by a SPP grating mode excited by z -polarization of the nano-disk illuminated under angled incident light.¹² A slight broadening of the experimental data compared with calculated values is also caused by this angled illumination.¹³ The overall agreement between experimental and calculated results indicates that the double-resonance structure has been fabricated as designed with high accuracy.

Figures 3(a) and 3(b) present cross-sectional images of the electric field distribution at 785 and 879 nm, respectively. For the calculation, P_x and P_y are set to 580 and 300 nm,

respectively, and the diameter and height of a nano-disk set to 130 and 30 nm, respectively. For both resonances, the electric field is significantly enhanced near the Au nano-disk. Furthermore, over the nano-disk, a large extensive evanescent field, which is a characteristic of SPP, is observed in Fig. 3(a).¹³

Figure 3(c) shows a contour plot of the electric field intensity at the position 2 nm above and 1 nm away from the edge of Au nanodisk (inset) as a function of P_y and the diameter. The electric field at the SPP resonance wavelength (~ 785 nm) and the LSP resonance one (~ 880 nm) is strongly enhanced especially when P_y is relatively large. When P_y is relatively small, e.g., smaller than ~ 300 nm, the field enhancement becomes small. This arises from the coupling between neighboring nanodisks, which leads to damping of surface plasmon resonances.²⁸ Figure 4(a) shows SERS spectra of 4-ATP on the double-resonance substrates with $P_x = 580$ nm and $P_y = 300$ nm (upper part). The nano-disk diameter is changed from 100 nm to 143 nm. For comparison, a normal Raman spectrum of 100- μm -thick 4-ATP formed by melting by heat and re-crystallizing by cooling is shown

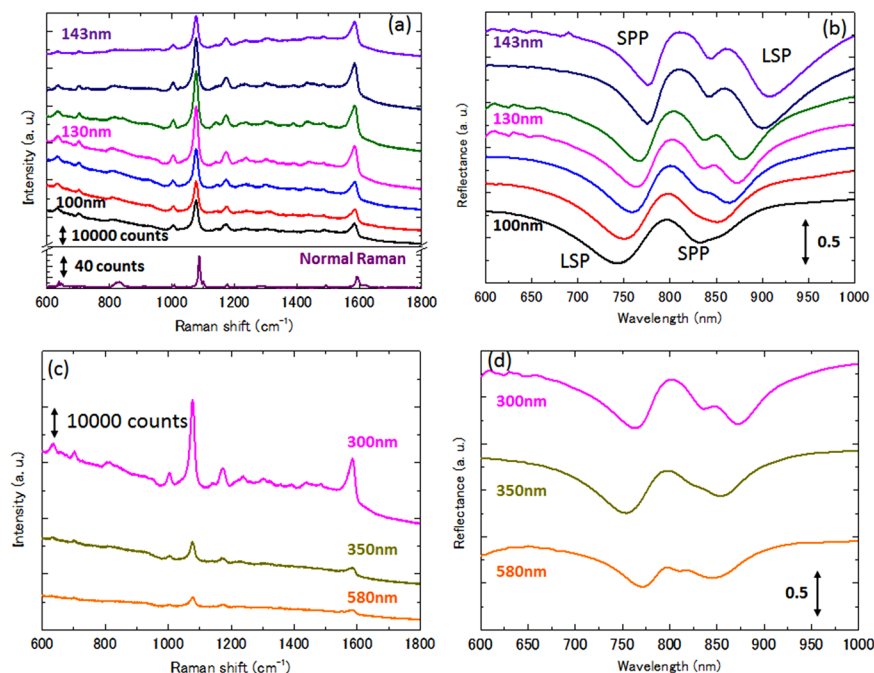


FIG. 4. (a) (Top panel) SERS spectra of 4-ATP on double-resonance nano-disk array substrates ($P_x = 580$ nm and $P_y = 300$ nm). For the spectra, the diameter changes from 100 to 143 nm. (Bottom panel) Normal Raman spectrum of 100 μm thick 4-ATP film. (b) Reflectance spectra corresponding to (a). (c) SERS spectra as P_y changes from 300 nm to 580 nm ($P_x = 580$ nm and diameter = 130 nm). (d) Reflectance spectra corresponding to (c).

at the bottom. The Raman signals at 1004, 1081, 1140, 1178, 1439, 1490, and 1589 cm^{-1} correspond to the vibration modes of $\nu_{\text{CC}}+\nu_{\text{CCC}}$ 18a(a₁), ν_{CS} 7a(a₁), δ_{CH} 9b(b₂), δ_{CH} 9a(a₁), $\nu_{\text{CC}}+\delta_{\text{CH}}$ 19b(b₂), $\nu_{\text{CC}}+\delta_{\text{CH}}$ 19a(a₁), and ν_{CC} 8a(a₁), respectively.²⁹ The Raman signals are strongly enhanced on the double-resonance substrates. As the diameter of nano-disks increases, the Raman signal at 1589 cm^{-1} with respect to that at 1080 cm^{-1} increases. This can be explained by the red-shift of the LSP resonance as diameter increases, as can be seen in the reflectance spectra in Fig. 4(b). The Raman signal at 1080 cm^{-1} is strongest when the diameter is 130 nm, arising through the almost exact coincidence of SPP and LSP resonance wavelengths with the excitation and Raman wavelengths.

In Figure 4(c), SERS spectra when P_y is changed from 300 nm to 580 nm and P_x and the diameter are fixed to 580 nm and 130 nm, respectively, are presented. The reflectance spectra of the same samples are shown in Fig. 4(d). The SERS signals monotonically increase with decreasing P_y , which is accompanied by a deepening in the reflectance dip in Fig. 4(d). These results indicate that the energy of the incident light is more effectively confined when P_y is smaller. However, this is not consistent with the result of the electric field simulation in Fig. 3(c). In the simulation, the field enhancement is the largest when P_y is 580 nm and decreases as P_y decreases. Since SERS EF is considered to be proportional to the EF of the electric fields at the excitation and Raman wavelengths,^{4,9} the simulation suggests the largest Raman EF when P_y is 580 nm. The reason for the discrepancy is not very clear at present, but may be caused by slightly different parameters between simulation and experiment,³⁰ e.g., incident angle and imperfection of the structure.

The SERS EF averaged over a laser spot is defined as $\text{EF} = (I_{\text{SERS}}/N_{\text{SERS}})/(I_{\text{NR}}/N_{\text{NR}})$,⁴ where I_{SERS} and I_{NR} are the intensities of a specific Raman line for SERS and normal Raman scattering, respectively. N_{SERS} and N_{NR} are the number of molecules in the laser spot for SERS and normal Raman scattering, respectively. In the present structure, N_{SERS} is calculated as $N_{\text{SERS}} = \rho_s S_{\text{gold}}A/(P_x \times P_y)$, where ρ_s is the 4-ATP surface packing density, S_{gold} is the surface area of one gold nanodisk, and A is the laser spot area.¹² N_{NR} is calculated using the volume density and molecular weight of 4-ATP, and the laser illumination volume, which is defined by the laser spot size and the penetration depth of the spot.³¹ The volume density, molecular weight, and surface packing density are 1180 kg/m^3 , 125.19, and $5 \times 10^{14}/\text{m}^2$,³¹ respectively. The average EF obtained for the optimized double-resonance substrate (P_x : 580 nm, P_y : 300 nm, diameter: 130 nm) in water is 7.8×10^7 . This value is among the highest in SERS substrates intended for use in biomedical and environmental applications.³²

In conclusion, through FDTD simulations and experiments, we have studied optimizing conditions to enhance responses of a double-resonance nano-disk array for NIR SERS in water. We showed high tunability of the SPP and LSP resonance wavelengths by changing the pitch and diameter of Au nano-disks. By the optimization of the SPP and

LSP resonance wavelengths, a maximum averaged NIR SERS EF of 7.8×10^7 can be achieved in water. We believe that SERS substrates of double-resonance nanodisk arrays can be used in biomedical or environmental applications that require SERS measurements in water in the NIR region.

M.S. would like to thank Professor. M. Fujii (Department of Electric and Electronic Engineering, Graduate School of Engineering, Kobe University, Japan) for his helpful discussions and comments.

- ¹K. Kneipp, Y. Wang, H. Kneipp, L. T. Perelman, I. Itzkan, R. R. Dasari, and M. S. Feld, *Phys. Rev. Lett.* **78**, 1667 (1997).
- ²M. Moskovits, *Rev. Mod. Phys.* **57**, 783 (1985).
- ³A. Otto, I. Mrozek, H. Grabhorn, and W. Akemann, *J. Phys.: Condens. Matter* **4**, 1143 (1992).
- ⁴E. C. Le Ru and P. G. Etchegoin, *Principles of Surface-Enhanced Raman Spectroscopy and Related Plasmonic Effects* (Elsevier, Amsterdam, 2009).
- ⁵J. M. Yuen, N. C. Shah, J. T. Walsh, Jr., M. R. Glucksberg, and R. P. Van Duyne, *Anal. Chem.* **82**(20), 8382 (2010).
- ⁶S. Shanmukh, L. Jones, J. Driskell, Y. P. Zhao, R. Dluhy, and R. A. Tripp, *Nano Lett.* **6**(11), 2630 (2006).
- ⁷M. Mulvihill, A. Tao, K. Benjathrit, J. Arnold, and P. Yang, *Angew. Chem. Int. Ed.* **47**, 6456 (2008).
- ⁸O. Péron, E. Rinnert, M. Lehaitre, P. Crassous, and C. Compère, *Talanta* **79**(2), 199 (2009).
- ⁹S. V. Gaponenko, *Phys. Rev. B* **65**, 140303(R) (2002).
- ¹⁰J. Cesario, R. Quidant, G. Badenes, and S. Enoch, *Opt. Lett.* **30**(24), 3404 (2005).
- ¹¹M. Kahl and E. Voges, *Phys. Rev. B* **61**(20), 14078 (2000).
- ¹²A. Ghoshal, I. Divliansky, and P. G. Kik, *Appl. Phys. Lett.* **94**, 171108 (2009).
- ¹³Y. Chu, M. G. Banaee, and K. B. Crozier, *ACS Nano* **4**(5), 2804 (2010).
- ¹⁴J. Petschulat, D. Cialla, N. Janunts, C. Rockstuhl, U. Hübner, R. Möller, H. Schneidewind, R. Mattheis, J. Popp, A. Tünnermann, F. Lederer, and T. Pertsch, *Opt. Express* **18**(5), 4184 (2010).
- ¹⁵J. Ye, M. Shioi, K. Lodewijks, L. Lagae, T. Kawamura, and P. Van Dorpe, *Appl. Phys. Lett.* **97**, 163106 (2010).
- ¹⁶R. A. Tripp, R. A. Dluhy, and Y. P. Zhao, *Nano Today* **3**(3–4), 31 (2008).
- ¹⁷A. Kaminska, O. Inya-Agha, R. J. Forster, and T. E. Keyes, *Phys. Chem. Chem. Phys.* **10**, 4172 (2008).
- ¹⁸R. Picorel, G. Chumanov, T. M. Cotton, G. Montoya, S. Toon, and M. Seibert, *J. Phys. Chem.* **98**, 6017 (1994).
- ¹⁹K. E. Shafer-Peltier, C. L. Haynes, M. R. Glucksberg, and R. P. Van Duyne, *J. Am. Chem. Soc.* **125**, 588 (2003).
- ²⁰V. Y. Lee, S. Farquharson, and P. M. Rainey, *Proc. SPIE* **3857**, 76 (1999).
- ²¹H. Schmidt, N. B. Ha, J. Pfannkuche, H. Amann, H. D. Kronfeldt, and G. Kowalewska, *Mar. Pollut. Bull.* **49**, 229 (2004).
- ²²*CRC Handbook of Chemistry and Physics*, 3rd electronic ed., edited by D. Lide (CRC Press, Boca Raton, FL, 2000).
- ²³*Handbook of Optical Constant of Solids*, edited by E. D. Palik (Academic Press, Orlando, FL, 1985).
- ²⁴P. B. Johnson and R. W. Christy, *Phys. Rev. Sect. B* **9**, 5056 (1974).
- ²⁵FDTD Solutions Reference Guide, Lumerical Solutions, Suite 300–535 Thurlow Street Vancouver, BC V6E 3L2, Canada, 2009.
- ²⁶K. Lodewijks, J. Ryken, W. Van Roy, G. Borghs, L. Lagae, and P. Van Dorpe, *Plasmonics* **8**, 1379 (2013).
- ²⁷Y. Chu, D. Wang, W. Zhu, and K. B. Crozier, *Opt. Express* **19**, 14919 (2011).
- ²⁸C. Sönnichsen, T. Franzl, T. Wilk, G. von Plessen, and J. Feldmann, *Phys. Rev. Lett.* **88**, 077402 (2002).
- ²⁹S. Guo, Y. Wang, and E. Wang, *Nanotechnology* **18**, 405602 (2007).
- ³⁰D. V. Guzatov, S. V. Vaschenko, V. V. Stankevich, A. Y. Lunevich, Y. F. Glukhov, and S. V. Gaponenko, *J. Phys. Chem. C* **116**, 10723 (2012).
- ³¹Y. Wang, H. Chen, S. Dong, and E. Wang, *J. Chem. Phys.* **124**, 074709 (2006).
- ³²M. Fan, G. F. S. Andrade, and A. G. Brolo, *Anal. Chim. Acta* **693**, 7 (2011).